Different DNA methylome, transcriptome and histological features in uterine fibroids with and without MED12 mutations

Ryo Maekawa (rmaekawa@yamaguchi-u.ac.jp)
Yamaguchi University Graduate School of Medicine

Shun Sato
Yamaguchi University Graduate School of Medicine

Tetsuro Tamehisa
Yamaguchi University Graduate School of Medicine

Takahiro Sakai
Yamaguchi University Graduate School of Medicine

Takuya Kajimura
Yamaguchi University Graduate School of Medicine

Kotaro Sueoka
Yamaguchi University Graduate School of Medicine

Norihiro Sugino
Yamaguchi University Graduate School of Medicine

Research Article

Keywords:

Posted Date: November 11th, 2021

DOI: https://doi.org/10.21203/rs.3.rs-1041773/v1

Different DNA methylome, transcriptome and histological features in uterine fibroids with and without MED12 mutations

Ryo Maekawa*, Department of Obstetrics and Gynecology, Yamaguchi University Graduate School of Medicine, Ube, 755-8505 Japan

Shun Sato, Department of Obstetrics and Gynecology, Yamaguchi University Graduate School of Medicine, Ube, 755-8505 Japan

Tetsuro Tamehisa, Department of Obstetrics and Gynecology, Yamaguchi University Graduate School of Medicine, Ube, 755-8505 Japan

Takahiro Sakai, Department of Obstetrics and Gynecology, Yamaguchi University Graduate School of Medicine, Ube, 755-8505 Japan

Takuya Kajimura, Department of Obstetrics and Gynecology, Yamaguchi University Graduate School of Medicine, Ube, 755-8505 Japan

Kotaro Sueoka, Department of Obstetrics and Gynecology, Yamaguchi University Graduate School of Medicine, Ube, 755-8505 Japan

Norihiro Sugino, Department of Obstetrics and Gynecology, Yamaguchi University Graduate School of Medicine, Ube, 755-8505 Japan

Corresponding author

Ryo Maekawa, M.D., Ph. D.*

Department of Obstetrics and Gynecology, Yamaguchi University Graduate School of Medicine, Ube, 755-8505 Japan

Phone : (+81)-836-22-2288

Fax : (+81)-836-22-2287

E-mail: rmaekawa@yamaguchi-u.ac.jp

Abstract

Background: Somatic mutations in Mediator complex subunit 12 (MED12m) have been reported as a biomarker of uterine fibroids (UFs). However, the role of MED12m is still unclear in the pathogenesis of UFs. Therefore, we investigated the differences in DNA methylome, transcriptome, and histological features between MED12m-positive and -negative UFs.

Methods: DNA methylomes and transcriptomes were obtained from MED12m-positive and -negative UFs and myometrium, and hierarchically clustered. Differentially expressed genes in comparison with the myometrium and co-expressed genes detected by weighted gene co-expression network analysis were subjected to gene ontology enrichment analyses. The amounts of collagen fibers and the number of blood vessels and smooth muscle cells were histologically evaluated.

Results: Hierarchical clustering based on DNA methylation clearly separated the myometrium, MED12m-positive, and MED12m-negative UFs. MED12m-positive UFs had the increased activities of extracellular matrix formation, whereas MED12m-negative UFs had the increased angiogenic activities and smooth muscle cell proliferation.

Conclusion: The MED12m-positive and -negative UFs had different DNA methylation, gene expression, and histological features. The MED12m-positive UFs form the tumor with a rich extracellular matrix and poor blood vessels and smooth muscle cells compared to the MED12m-negative UFs, suggesting MED12 mutations affect the tissue composition of UFs.

Introduction

Uterine fibroids are tumors derived from uterine smooth muscle cells and are most common in gynecologic neoplasms [1]. In the last decade, somatic mutations of Mediator complex subunit 12 (MED12) have been found to be reliable biomarkers of uterine fibroids [2-4]. MED12 is located on the X chromosome and encodes the RNA polymerase II mediator complex and part of the transcriptional preinitiation machinery. Mutations of MED12, especially mutations in exon 2, are thought to be the underlying causes of about 70% of human uterine fibroids [2,5,6]. However, the remaining 30% of uterine fibroids do not have MED12 mutations, which indicates that the role of MED12 mutations in the pathogenesis of uterine fibroids is unclear.

Uterine fibroids differ in size and the number of nodules. Uterine fibroids carrying MED12 mutations are reported to be smaller and often more numerous than those without MED12 mutations [4]. Several reports have suggested links between MED12 mutations and different phenotypes of uterine fibroids. Uterine fibroids without MED12 mutations were found to have elevated erythropoietin expression in an estrogen-dependent manner, while the uterine fibroids with MED12 mutation had low erythropoietin [7,8]. Furthermore, uterine fibroids with and without MED12 mutations had different cell components and different amounts of collagen [9]. These reports suggest that MED12 mutations are associated with different phenotypes of uterine fibroids. On the other hand, genome-wide gene expression profiles were not different between uterine fibroids with and without MED12 mutations [10]. A comparison of transcriptomes from uterine fibroids with and without MED12 mutations found difference in only a few specific intracellular signaling-pathways including arachidonic acid metabolism [11]. Thus, it remains unclear whether uterine

65 fibroid phenotypes are associated with MED12 mutations.

66 DNA methylation is a major type of epigenetic mark. DNA methylation profiles define each type
67 of normal cells and distinguish cell types [12-14], and therefore have been used to characterize abnormal cells
68 [13,14]. DNA methylation is tissue/cell-specific, and DNA methylation profiling is more useful than profiling
69 mRNA expression to define the cell identity [15]. We previously reported that uterine fibroids had different
70 DNA methylation profiles from normal myometrium by genome-wide approach and that DNA methylation
71 profiles segregated the uterine fibroids and normal myometrium [15,16]. Furthermore, using these differently
72 methylated genes between uterine fibroids and normal myometrium, we found some potential mechanisms
73 for the pathogenesis of uterine fibroids [15-19]. We also found significant differences in DNA methylation
74 levels of those genes between uterine fibroids with and without MED12 mutations [16]. These findings led
75 us to investigate differences in genome-wide DNA methylation profiles between uterine fibroids with and
76 without MED12 mutations.

77 We recently identified SATB2 and NRG1 as potential upstream regulatory factors in uterine
78 fibroids [19]. SATB2 and NRG1 expressions were increased in uterine fibroids compared to the myometrium.
79 Both SATB2 and NRG1 activated WNT/beta-catenin and TGF-beta signaling pathways, which are related
80 to the pathogenesis of uterine leiomyomas [19]. Interestingly, established cell lines overexpressing SATB2
81 morphologically changed from spindle-like forms to fibroblast-like forms with elongated protrusions [19],
82 suggesting that SATB2 and NRG2 play essential roles in initiating tumorigenesis in uterine fibroids.
83 However, the association between the expression of NRG1 and SATB2, and MED12 mutations is still unclear.

In the present study, we examined the associations between MED12 mutations and four aspects of uterine fibroids: 1) genome wide methylation profiles, 2) cellular functions as revealed by transcriptome analyses, 3) different histopathological features and 4) the expressions of NRG1 and SATB2.

Results

Hierarchical clustering using DNA methylation profiles

We first examined the DNA methylome of the uterine fibroids with and without MED12 mutations (MED12m-positive uterine fibroids (n = 6) and MED12m-negative uterine fibroids (n = 12), respectively), and myometrium (n = 6). Hierarchical clustering showed that the myometrium made a distinct cluster from uterine fibroids (Fig. 1a). The MED12m-positive and -negative uterine fibroids were classified into different clusters (Fig. 1a), suggesting that uterine fibroids with and without MED12 mutations are different at the molecular levels.

The MED12m-positive uterine fibroids were clearly clustered, while the MED12m-negative uterine fibroids can be further classified into three clusters (Subtype-1, -2, and -3; Fig. 1a). Subtype-1 was classified into the same cluster as the MED12m-positive uterine fibroids (Fig. 1a). Subtypes-2 and -3 were classified into clusters different from Subtype-1 (Fig. 1a).

Figure 1b shows the distribution of aberrantly methylated CpGs in the MED12m-positive and -negative uterine fibroids compared to the myometrium throughout the chromosomes. The results showed that the DNA methylation statuses of Subtype-1 are similar to that of the MED12m-positive uterine fibroids.

On the other hand, in Subtypes-2 and -3, the DNA methylation status in the autosomes tended to be hypermethylated compared to that in Subtype-1 and the MED12-positive uterine fibroids (Fig. 1a).

Differentially expressed genes (DEGs)

We determined DEGs in the MED12m-positive and -negative uterine fibroids compared to the myometrium. The MED12m-positive fibroids had 157 increased and 233 decreased genes compared to the myometrium (Supplemental Tables S1 and S2 online). The MED12m-negative fibroid had 110 increased and 207 decreased genes compared to the myometrium (Supplemental Tables S3 and S4 online). The DEGs were subjected to the GO enrichment analysis to know the characteristics of the DEGs.

The GO terms "telomere organization", "DNA replication-dependent nucleosome assembly", "positive regulation of gene expression epigenetic", "extracellular matrix organization", "collagen catabolic process", "cell adhesion", "integrin-mediated signaling pathway", "cellular protein metabolic process", "response to estrogen", and "canonical Wnt signaling pathway" were detected in the increased genes in the MED12m-positive uterine fibroids (Fig. 2a). In the decreased genes in the MED12m-positive uterine fibroids (Fig. 2b), the GO terms "reactive oxygen species metabolic process", "inflammatory response", "regulation of inflammatory response", "angiogenesis", "regulation of macrophage activation", and "positive regulation of apoptotic process" were detected.

In the MED12m-negative uterine fibroids, the GO terms "cellular protein metabolic process", telomere organization", DNA replication-dependent nucleosome assembly", "positive regulation of gene

122 expression epigenetic", "liver regeneration", and "negative regulation of canonical Wnt signaling pathway"
123 were detected in the increased genes (Fig. 2d). In the decreased genes in the MED12m-negative uterine
124 fibroids (Fig. 2d), the GO terms "cell adhesion", "extracellular matrix organization", "positive regulation of
125 cell-substrate adhesion", "integrin-mediated signaling pathway", "negative regulation of transcription by
126 RNA polymerase II", "inflammatory response", "reactive oxygen species metabolic process", "positive
127 regulation of apoptotic process", and "transforming growth factor-beta receptor signaling pathway" were
128 detected.

129 Figure 2e summarizes the results of GO enrichment analyses of DEGs. Compared to
130 myometrium, MED12m-positive uterine fibroids showed increased activities of extracellular matrix
131 organization, cell adhesion, integrin-mediated signaling, and Wnt signaling pathway, whereas MED12m-
132 negative uterine fibroids had the decreased activities of them and TGF-beta signaling, suggesting that
133 MED12m-positive uterine fibroids have the increased activity of extracellular matrix formation compared
134 with MED12m-negative uterine fibroids. In addition, MED12m-positive uterine fibroids showed the
135 increased responsiveness to estrogen and decreased angiogenic activities. Both types of uterine fibroids
136 had increased cell proliferation and transcription activities and decreased inflammatory response and
137 reactive oxygen species metabolic process activities compared to myometrium. Figure 3 shows the
138 expression statuses of representative genes of the commonly (Fig. 3a) and oppositely (Fig. 3b) regulated
139 processes between the MED12m-positive and MED12m-negative uterine fibroids.

140

Weighted gene co-expression network analysis (WGCNA)

The preceding DEGs (Fig. 2) is based on comparing the uterine fibroids with the myometrium, and this analytic approach has been used so far [10,11]. In general, in the analytic method that compares the target tissues to the control tissues, there is a possibility of missing the essential character of the target tissue when the cell character of the target tissue is close to that of the control tissue. Therefore, to know the intrinsic character in each of the MED12m-positive and -negative uterine fibroids, we used a WGCNA analysis [20,21]. WGCNA is a system biology method to describe the correlation patterns among the genes across microarray samples such as transcriptome data and to find the groups with highly correlated genes that work in the same biological functions [20,21]. We defined groups consisting of highly correlated genes as co-expressed gene (COG) groups and detected unique properties in the MED12m-positive and -negative uterine fibroids by comparing the intrinsic functions of each tissue.

The transcriptome data of the MED12m-positive and -negative uterine fibroids were independently subjected to the WGCNA. In the MED12m-positive and -negative uterine fibroids, WGCNA identified 26 and 14 COG groups, respectively (Table 1), and these genes were subjected to the GO enrichment analysis.

In the MED12m-positive uterine fibroids, three of the 26 COG groups had significant GO terms, while in the MED12m-negative uterine fibroids, five of the 14 COGs groups had significant GO terms (Table 1). Figure 4 shows the specific GO terms from three COG groups in the MED12m-positive (Group1, Group2, and Group3) and five COG groups in the MED12m-negative (Group1, Group2, Group3, Group4,

and Group5), respectively. The commonly detected GO terms between the MED12m-positive and -negative uterine fibroids included "RNA splicing, via transesterification reactions", "mRNA splicing, via spliceosome", ncRNA processing", "mRNA processing", and "RNA splicing", which are related to transcription and translation, and "ribonucleoprotein complex biogenesis" and "DNA replication", which are related to cell proliferation (Fig. 4).

The extracellular matrix-related terms including "extracellular structure organization" and "extracellular matrix organization" were also commonly found. The gene ratios were much larger in the MED12m-positive uterine fibroids than those in the MED12m-negative uterine fibroids, suggesting that the number of extracellular matrix-related genes was larger in the MED12m-positive uterine fibroids than that in the MED12-negative uterine fibroids (Fig. 4).

We then focused on specific GO terms in each of the MED12m-positive or -negative uterine fibroids. There were no specific GO terms to the MED12m-positive uterine fibroids (Fig. 4). On the other hand, the MED12m-negative uterine fibroids had specific GO terms related to cellular protein synthesis ("Golgi vesicle transport", "ER to Golgi vesicle-mediated transport", and "Rho protein signal transduction"), anti-apoptosis ("regulation of apoptotic signaling pathway"), muscles ("muscle system process" and "muscle contraction", and "mitochondrial ATP synthesis coupled electron transport"), and angiogenesis ("blood vessel morphogenesis", "angiogenesis", "regulation of vasculature development", and regulation of angiogenesis") (Fig. 4).

These WGCNA results suggest that MED12m-positive uterine fibroids have an increased activity

of extracellular matrix organization compared with MED12m-negative uterine fibroids. On the other hand, MED12m-negative uterine fibroids showed increased activities of angiogenesis and smooth muscle cell proliferation. Both types of uterine fibroids had increased activities of cell proliferation and transcription for gene expression.

Immunofluorescence staining

The GO enrichment analysis in the DEGs and COG groups indicated that the MED12m-positive uterine fibroids have increased activities of extracellular matrix organization and that the MED12m-negative uterine fibroids have increased activities of angiogenesis and proliferation of smooth muscle cells (Figs. 2 and 4). We histologically examined the amount of collagen fibers in the MED12m-positive and -negative uterine fibroids, and myometrium. Immunofluorescence staining showed that the amount of collagen fibers was significantly larger in the MED12m-positive uterine fibroid than in the myometrium and MED12m-negative fibroids (Fig.5a and 5b). There was no significant difference between the myometrium and MED12m-negative uterine fibroids. We next examined the number of blood vessels in the MED12m-positive and -negative uterine fibroids, and myometrium. The result showed that the number of blood vessels was significantly higher in the MED12m-negative uterine fibroids than in the MED12m-positive uterine fibroids (Fig. 5c and 5d). There was no significant difference between the MED12m-negative uterine fibroids and myometrium. We also examined the ratio of smooth muscle cells in total cells in the MED12m-positive, -negative uterine fibroids, and myometrium. The percentage of smooth muscle cells

198 was significantly higher in the MED12m-negative uterine fibroids than the MED12m-positive uterine
199 fibroids and myometrium (Fig. 5e and 5f). There was no significant difference between the MED12m-
200 positive uterine fibroids and myometrium.

201

202 *Upstream regulators in uterine fibroids*

203 To know whether mutations in MED12 are associated with the upregulation of upstream regulators,
204 SATB2 and NRG1 in uterine fibroids, we examined the DNA methylation and expression levels of SATB2
205 and NRG1 in the uterine fibroids with and without MED12 mutations. In SATB2, 88.9% (8 of 9 samples)
206 of the MED12m-positive uterine fibroids and 75% (9 of 12 samples) of the MED12m-negative uterine
207 fibroids showed higher DNA methylation levels (more than 15% DNA methylation) than the myometrium,
208 respectively (Fig. 6a and Supplemental Table S5 online). In NRG1, 100% (9 of 9 samples) of the
209 MED12m-positive uterine fibroids and 75% (9 of 12 samples) of the MED12m -negative uterine fibroids
210 showed higher DNA methylation levels than the myometrium, respectively (Fig. 6b and Supplemental Table
211 S5 online).

212 The mRNA expression levels of SATB2 in all nine of the MED12m-positive uterine fibroids and 75%
213 (9 of 12 samples) of the MED12m-negative uterine fibroids were more than twice those in the myometrium
214 (Fig. 6c and Supplemental Table S5 online), while the mRNA expression levels of NRG1 in all the
215 MED12m-positive uterine fibroids and 67% (8 of 12 samples) of the MED12m-negative uterine fibroids
216 were more than twice those in the myometrium, (Fig. 6d and Supplemental Table S5 online). DNA

methylation and mRNA expression of at least one of SATB2 and NRG1 were higher in all the MED12m-positive and -negative uterine fibroids than they were in the myometrium. Since DNA hypermethylation and increased expression of SATB2 or NRG1 were observed regardless of MED mutations, these characteristics are unlikely to depend on MED12 mutations.

Discussion

The present study showed that the DNA methylation profiles of the MED12m-positive and -negative uterine fibroids differed. Since DNA methylation is cell/tissue-specific, uterine fibroids with MED12 mutations differ from uterine fibroids without MED12 mutations at the molecular level. This prompted us to clarify the difference between the two types of uterine fibroids in this study.

In the MED12m-positive uterine fibroids, DEGs were enriched to the GO terms related to extracellular matrix organization. The WGCNA analysis also showed the activated extracellular matrix organization in the MED12m-positive uterine fibroids. On the other hand, in the MED12m-negative uterine fibroids, most of the genes in the GO terms related to extracellular matrix organization were down-regulated in comparison with the myometrium and MED12m-positive uterine fibroids. Furthermore, the TGF-beta signaling pathway, which contributes to fibrosis [22,23], was downregulated in the MED12m-negative uterine fibroids. These results suggest that MED12 mutations activate extracellular matrix organization in uterine fibroids. In fact, our histological results showed that the amount of collagen was enriched in the uterine fibroids with MED12 mutations. Many reports have shown the increased expression of COL4A1 and COL4A2, which

236 contribute to collagen synthesis, and increased collagen deposition in uterine fibroids [11,24]. Also, many of
237 the uterine fibroids in those studies may have been MED12m-positive because more than 70% of uterine
238 fibroids are MED12m-positive.

239 The WGCNA analysis in the MED12m-negative uterine fibroids detected a COGs group that is related
240 to muscles. In our histological results, the amount of smooth muscle cells was larger in the uterine fibroids
241 without MED12 mutations compared with the uterine fibroids with MED12 mutations, which is consistent
242 with a previous report demonstrating a high ratio of smooth muscle cells to fibroblasts in the uterine fibroids
243 without MED12 mutations compared to that with MED12 mutations [9]. That study, together with the present
244 results suggest that uterine fibroids without MED12 mutations are enriched in smooth muscle cells and
245 contain a low amount of collagen fibers, and that MED12 mutations are associated with collagen-rich uterine
246 fibroids.

247 The GO enrichment analyses with DEGs and WGCNA analysis showed that both MED12m-
248 positive and -negative uterine fibroids have increased cell proliferation and transcription activities. This
249 well reflects one of the characters of uterine fibroids, which is the activated cell proliferation of smooth
250 muscle cells or fibroblasts. It is interesting to note that the activity of the Wnt signaling pathway was
251 decreased in MED12m-negative uterine fibroids. The Wnt signaling pathway has been reported to play an
252 important role in the growth of uterine fibroids [22]. This may be because the major type of uterine fibroids
253 included in those reports was MED12m-positive uterine fibroids in which Wnt signaling pathway is activated.
254 We speculate that the growth of MED12m-negative uterine fibroids is regulated by signaling pathways other

than the Wnt signaling pathway. As shown in Table 2, multiple signaling pathways are involved in cell proliferation in both MED12m-positive and -negative uterine fibroids.

VEGF expression is reported to be upregulated in uterine fibroids [25], which suggests that angiogenic activity in increased in uterine fibroids. On the other hand, our GO enrichment analysis suggested that angiogenesis is downregulated in MED12m-positive uterine fibroids and upregulated in MED12m-negative uterine fibroids. There seems to be a discrepancy between the previous reports and our results. That may be due to the difference in cellular components of the tissue samples of uterine fibroids. As shown in the histological features of both types of uterine fibroids, MED12m-positive uterine fibroids are collagen-rich while MED12m-negative uterine fibroids are cell-rich. Collagen-rich tissues should show low angiogenesis while cell-rich tissues should show high angiogenic activity. In fact, our result indicated that the MED12m-negative uterine fibroids had higher number of blood vessels compared with the MED12m-positive uterine fibroids.

In addition, the response to estrogen was found to be upregulated in MED12m-positive uterine fibroids. Since fibroblasts were reported to proliferate or produce collagen in response to estrogen while smooth muscle cells proliferate in response to progesterone [9], collagen-rich MED12m-positive uterine fibroids seem to well respond to estrogen.

Our results also suggested that the immune response and reactive oxygen species metabolic processes are decreased in both MED12m-positive and -negative uterine fibroids. That is not surprising because tumorigenesis is well known to occur under the suppressive environment of immune responses and

reactive oxygen species [25 26 27,28].

High mobility group AT-hook2 (HMGA2) mutation is considered to be one of the mutations driving the development of uterine fibroids [3,29,30], and the MED12 mutations and rearrangement of HMGA2 have been shown to occur in a mutually exclusive manner [4,5]. However, our results showed that some uterine fibroids carried both the MED12 mutation and HMGA2 overexpression, and that only half of the MED12m-negative fibroids had increased HMGA2 expression (Supplemental Fig. S2). Previous reports also indicated that the MED12 mutations and increased HMGA2 expression co-existed in the same uterine fibroid nodule [10,31].

We previously reported that SATB2 and NRG1 act as upstream regulatory factors in the pathogenesis of uterine fibroids [19,22,23]. Whether or not MED12 has a mutation, SATB2 and NRG1 were more strongly expressed in uterine fibroids than in the myometrium, which indicates that the upregulation of NRG1 and SATB2 are independent of MED12 mutations. Our results also indicated that all the MED12m-positive and -negative uterine fibroids had DNA hypermethylation and increased mRNA expression in either SATB2 or NRG1, suggesting that the dysregulation of upstream regulatory factors such as SATB2 and NRG1 is involved in the pathogenesis of uterine fibroids.

One may question the relationship between MED12 mutation and DNA methylation; whether MED 12 mutation changes DNA methylation status. It is unlikely that a MED 12 mutation could change the DNA methylation status because the DNA methylation profile of subtype-1 MED12m-negative uterine fibroids was identical to the MED12m-positive uterine fibroids. Further studies are needed to identify the

differences among the three subtypes of uterine fibroids without MED12 mutation.

In conclusion, the present study shows that uterine fibroids with and without MED12 mutations clearly differ in DNA methylation, gene expression, and histological features. The DNA methylome indicated that the uterine fibroids carrying MED12 mutations differed from the uterine fibroids without MED12 mutations, and that MED12 mutations do not directly change DNA methylation profiles of uterine fibroids. The transcriptome and histological examination revealed that the MED12m-positive uterine fibroids increased extracellular matrix production activity compared with the MED12m-negative uterine fibroids. MED12 mutations may affect the phenotypes of uterine fibroids by modulating the production of extracellular matrix. Both types of uterine fibroids had increased cell proliferation activities, but they may use different signaling pathways for growth. The present study shows that uterine fibroids differ depending on the presence of MED12 mutations.

Methods

Ethics Statement

This study was reviewed and approved by the Institutional Review Board of Yamaguchi University Graduate School of Medicine. Written informed consent was obtained from the participants before collecting any samples, and the specimens were irreversibly de-identified. All experiments involving the handling of human tissues were performed following the Tenets of the Declaration of Helsinki.

311

312 *Tissue preparation*

313 Tissues of uterine fibroid and myometrium were obtained from 42 Japanese women, respectively.
314 Uterine fibroids were obtained from patients aged 33-45 who underwent hysterectomy for uterine fibroids.
315 Myometrium was obtained from patients with uterine fibroids aged 34-42 who underwent hysterectomy for
316 uterine fibroids or early stage of cervical cancer. None of the women enrolled in this study received
317 previous treatment with sex steroid hormones or gonadotropin-releasing hormone agonists/antagonists.
318 We analyzed the uterine fibroids with MED12 mutation status by Sanger sequencing as reported previously
319 (Supplemental Fig. S1 online) [16]. All of the MED12m-positive uterine fibroids had the point mutations in
320 MED12 gene. MED12 expression levels were not significantly different between myometrium and uterine
321 fibroids with or without MED12 mutation.

322

323 *HMGA2 expression statuses*

324 HMGA2 rearrangements are thought to be one of the mutations driving the development of uterine
325 fibroids [3,30]. Among the uterine fibroids without MED12 mutations, uterine fibroids carrying HMGA2
326 rearrangements oocur with the highest frequency [3,30]. More than 80% of uterine fibroids possess karyotypic
327 abnormalities, and MED12 mutations and HMGA2 rearrangements encompass approximately 80-90% of
328 genetic alterations in uterine fibroids [3,29,30]. Previous reports indicated that the MED12 mutations and
329 rearrangement of HMGA2 occur in a mutually exclusive manner [4,5]. Therefore, it has been suggested that

330 the MED12 mutations and HMGA2 rearrangements were alternatively associated with the pathogenesis of
331 uterine fibroids. Hence, past reports compared the features between the uterine fibroids with the MED12
332 mutations and that with HMGA2 rearrangements [9,10]. The uterine fibroids carrying HMGA2
333 rearrangement are reported to overexpress HMGA2 [10]. To investigate whether our samples included the
334 uterine fibroids carrying HMGA2 rearrangement, we examined the expression levels of HMGA2 in the
335 MED12m-negative and MED12m-positive uterine fibroids, and myometrium using transcriptome analyses.
336 Three of the nine MED12m-negative uterine fibroids had expressions more than two-fold of the mean
337 expression in the myometrium (Supplemental Fig. S2 online). Moreover, one of the six MED12m-positive
338 uterine fibroids had expressions more than two-fold of the mean expression in the myometrium
339 (Supplemental Fig. S2 online). These results suggest that 1) a number of the MED12m-negative uterine
340 fibroids lack HMGA2 rearrangements, and 2) MED12 mutations and HMGA2 rearrangements can co-exist.
341 These facts led us to compare the uterine fibroids with and without MED12 mutations rather than to compare
342 uterine fibroids with MED12 mutations and HMGA2 rearrangements.
343
344 *Illumina Infinium HumanMethylation450 BeadChip Assay*
345 Genomic DNA was isolated from the uterine fibroids and myometrium using a Qiagen Genomic
346 DNA kit (Qiagen, Valencia, CA, USA), as previously reported [32]. DNA methylation was analyzed with an
347 Illumina Infinium assay with the HumanMethylation450 BeadChip (Illumina, San Diego, CA, USA), which
348 interrogates a total of 482,421 CpGs spread across the distal promoter regions of the transcription start sites

to 3'-UTR of consensus coding sequences. Methylated and unmethylated signals were used to compute beta-values, which are quantitative scores of the DNA methylation levels, ranging from 0 (completely unmethylated) to 1 (completely methylated). The BeadChip was scanned on a BeadArray Reader (Illumina) according to the manufacturer's instructions. CpGs with "detection p values">0.01 (computed from the background based on negative controls), CpGs that were zero in all samples, and CpGs on Y chromosome were eliminated from further analysis, leaving 422,165 CpGs valid for use. The DNA methylation data of the CpGs were normalized in genome studio. We used NCBI Reference Sequence Database (https://www.ncbi.nlm.nih.gov/refseq/) as reference genes.

Transcriptome analysis

The transcriptomes of myometrium, MED12m-positive, and -negative uterine fibroids were analyzed as previously reported [33,34]. Total RNAs were isolated from cells by using an RNeasy mini kit (Qiagen). Target cDNA for a microarray was prepared from 250 ng of total RNA with the Ambion WT Expression kit (Ambion, Austin, TX, USA) and the GeneChip WT PLUS reagent kit (Affymetrix). Transcriptomes were analyzed with a GeneChip Human Genome 1.0 ST Array (Affymetrix, Santa Clara, CA, USA) as previously reported [33,34]. The microarray was spotted with 21,014 RefSeq genes. Hybridization to the microarrays, washing, staining, and scanning was performed using the GeneChip system (Affymetrix) composed of the Scanner 30007 G Workstation Fluidics 450 and the Hybridization Oven 645. The scanned image data were processed using a gene expression analysis with the Patrek

Genomics Suite 6.5 software program (Partech, Munster, Germany). All expression data were converted to log2 values. Differentially expressed genes (DEGs) were extracted when the expressions in the MED12m-positive or -negative uterine fibroids were higher than 2.0-fold or less than 0.5-fold of that in the myometrium, and $p < 0.05$ (t-test), and the average expression levels in the tissues with higher expression were more than 100.

Weighted gene co-expression network analysis (WGCNA)

We employed a weighted gene co-expression network analysis (WGCNA) package in R [20,21] according to the manufacturer's instructions to identify genes that were co-expressed in uterine fibroids and myometrium. Low signal probes with values < 10 in more than 90% of the samples were considered as noise and removed, and correlations based on mostly zero counts are not meaningful. To stabilize the samples' variance, we used the variance stabilizing transformation function in DESeq2 [35]. The blockwise-Module function was used with the parameters; power = 12; minimum module size = 50; deep split = 0; cut height = 0.95; gene group merge height = 0.25. Detected gene groups were subjected to gene annotation analysis using clusterProfiler in R [36]. The ratio of the number of identified genes to all genes in each term was calculated. P-values were adjusted by the Benjamini and Hochberg (BH) method that is the default p-value adjustment in clusterProfiler [36].

Immunohistochemistry

Collagen fibers were stained and visualized in tissue sections using the Trichrome Stain Kit (TRM-1, ScyTec Laboratories inc., Utah, USA) following the manufacturer's instructions. Tissue sections (5μm) of paraffin-embedded samples were deparaffinized, washed with cold phosphate-buffered saline (PBS), placed in preheated Bouin's fluid overnight, rinsed in tap water until completely clear, rinsed in distilled water, stained with Weigert's Iron Hematoxylin for 10 minutes, rinsed in tap water for 2 minutes, rinsed in distilled water, immersed in Biebrich Scarlet/Acid Fuchsin Solution for 10 minutes, rinsed in distilled water, defferentiated in Phosphomolybdic/Phosphotungstic Acid Solution for 15 minutes, placed in Aniline Blue Solution for 15 minutes, rinsed in distilled water, immersed in Acetic Acid Solution (1%) for 1 minute, dried, placed in Xylene 3 times and mounted in synthetic resin. The area of collagen fibers, which were stained blue, was quantified by Image J, and the percentage per field of view was calculated. The calculations were done on 15 randomly chosen areas at x200, and the average percentages were used as the collagen fiber area (%) in each tissue.

Tissue sections (5μm) of paraffin-embedded samples were deparaffinized, washed with cold phosphate-buffered saline (PBS), and blocked with blocking solution (10% bovine fetal serum and 1% bovine serum albumin in PBST) for 60 min. Then the cells were incubated with mouse anti-αSMA monoclonal antibody for smooth muscle cell staining (Abcam, Tokyo, Japan; Cat# ab7817, RRID: AB_262054) and rabbit anti-CD31 monoclonal antibody for vascular endothelial cells (Abcam, Cat# ab182981, RRID: AB_2756834) as primary antibody (diluted at 1:500 in the blocking solution) at 4 C overnight, and incubated with the Alexa Fluor 488 or 594 conjugated goat anti-mouse IgG (Abcam, Cat#

406 ab150113: RRID: AB_2576208; Abcam, Cat# ab150116: RRID: AB_2650601) and the Alexa Fluor 594
407 conjugated goat anti-rabbit IgG (Abcam, Cat# ab150084, RRID: AB_2734147) as secondary antibodies
408 (diluted at 1:1000 in PBS) for 45 min a room temperature, respectively. The number of blood vessels,
409 which were stained red larger than 15 pixels, was counted by Image J, and the number per field of view was
410 calculated. The calculations were done on 5 randomly chosen areas at x100, and the average numbers were
411 used in each tissue. The percentages of smooth muscle cells were calculated as follows: the number of
412 smooth muscle cells/the number of smooth and non-smooth muscle cells. Cells stained with or without
413 αSMA were considered as smooth muscle cells or non-smooth muscle cells. The number per view field
414 was calculated on 5 randomly chosen areas at x200 magnification, and the average numbers were indicated
415 in each tissue section.

416 The amounts of collagen fibers, the number of blood vessels, and the percentage of smooth muscle
417 cells between the MED12m-positive and -negative uterine fibroids and myometrium were compared with
418 pairwise Wilcoxon rank-sum tests using R (function "pairwise.wilcox.test"; version 3.6.0.). $p < 0.05$ was
419 considered significant.

420

421 *Bioinformatics*

422 DAVID Bioinformatics Resources v. 6.8 (https://david.ncifcrf.gov/) and Ingenuity Pathway
423 Analysis (IPA, Qiagen) were used to determine whether the functional annotation of the differentially
424 expressed genes was enriched for specific Gene Ontology (GO) terms and biological pathways (Kyoto

425 Encyclopedia of Genes and Genomes; KEGG), respectively [37]. In GO analysis, GO terms with adjusted p
426 (BH method) < 0.01 were considered significant enrichment. In KEGG analysis, pathways with $p < 0.05$
427 were considered significant enrichment. In WGCNA analysis, adjusted $p < 0.1$ was regarded as substantial
428 enrichment in the GO enrichment analysis. Hierarchical clustering was performed in R using the Ward
429 method [38]. Chromosomal distributions of the DNA methylation statuses of all CpG loci in the MED12m-
430 positive and -negative uterine fibroids compared to the myometrium were examined using "chromoMap"
431 implemented in R (https://cran.r-project.org/web/packages/chromoMap/index.html). CpG sites, which
432 have $p<0.05$ and beta-value difference >0.2 compared to the myometrium, are plotted in autosomes and X
433 chromosome. The GO terms were summarized by removing redundancy and plotted using reduce and
434 visualize gene ontology (REVIGO) with Allowed Similarity as "small (0.5)" [39].
435
436 *Combined Bisulfite Restriction Analysis (COBRA)*
437 DNA methylation levels were evaluated by COBRA as we previously reported [15,16]. In brief,
438 sodium bisulfite treatment was performed using an EpiTect Bisulfite kit (Qiagen) according to the conditions
439 as follows: 95 °C for 5 min, 65 °C for 85 min, 95 °C for 5 min and 65 °C for 175 min. After sodium
440 bisulfite treatment, PCR was performed using one unit of Biotaq HS DNA polymerase (Bioline, London,
441 UK) and the primer sets shown in Supplemental Table S6 online under the thermocycling conditions (35 to
442 38 cycles of 95 °C for 30 sec, 60 °C for 30 sec, and 72 °C for 30 sec, with an initial step of 95 °C for 10 min
443 and a final step of 72 °C for 7 min). A part of the PCR product was digested with the restriction enzyme

444 TaqI (Takara, Tokyo, Japan) or HpyCH4IV (New England Biolabs, Ipswich, MA). The treated PCR
445 product was electrophoresed by 3% agarose gel. PCR products from methylated DNA and unmethylated
446 DNA are digested and undigested by the treatment with the restriction enzyme. The intensity of the signals
447 of the digested and undigested PCR products was measured by densitometry. Methylation levels (%) were
448 calculated as the ratio of the digested PCR product in the total PCR product (digested + undigested products).
449
450 *Quantitative real-time RT-PCR (qRT-PCR)*
451 Total RNA was isolated from tissues and cells using Isogen (Wako Pure Chemical Industries Ltd,
452 Osaka, Japan). One μg total RNA was reverse-transcribed using a Quantitect Reverse Transcription Kit
453 (Qiagen) according to the manufacturer's protocol as previously reported [15]. A primer pair for
454 glyceraldehyde-3-phosphate dehydrogenase (*GAPDH*) was used as an internal control. Real-time qRT-
455 PCR was performed using SYBR Premix Ex Taq (Takara, Ohtsu, Japan) and a LightCycler (Roche Applied
456 Science, Basel, Switzerland). All samples were run in duplicate. The relative quantity of cDNA was
457 calculated with the ΔΔCt method. Melting curves of the products were obtained after cycling by a stepwise
458 increase of temperature from 55 to 95 °C. The primer sequences used in this analysis are shown in
459 Supplemental Table S6 online.
460
461 *Statistical analysis*
462 All statistical analyses were performed in R [38].

Computing platform

The computing platform used in this study was an Intel(R) Xeon(R) CPU E5-2667 v4, 3.20GHz (x 4 CPUs, eight cores per CPU) with 504GB RAM running CentOS release 6.10.

References

1 Stewart, E. A. Uterine fibroids. *Lancet* **357**, 293-298 (2001).

2 Makinen, N. *et al.* MED12, the mediator complex subunit 12 gene, is mutated at high frequency in uterine leiomyomas. *Science* **334**, 252-255 (2011).

3 Mehine, M. *et al.* Characterization of uterine leiomyomas by whole-genome sequencing. *N Engl J Med* **369**, 43-53 (2013).

4 Bullerdiek, J. & Rommel, B. Factors targeting MED12 to drive tumorigenesis? *F1000Res* **7**, 359, doi:10.12688/f1000research.14227.2 (2018).

5 Markowski, D. N. *et al.* MED12 mutations in uterine fibroids--their relationship to cytogenetic subgroups. *Int J Cancer* **131**, 1528-1536 (2012).

6 Mittal, P. *et al.* Med12 gain-of-function mutation causes leiomyomas and genomic instability. *J Clin Invest* **125**, 3280-3284 (2015).

7 Asano, R. *et al.* Aberrant expression of erythropoietin in uterine leiomyoma: implications in tumor growth. *Am J Obstet Gynecol* **213**, 199 e191-198, doi:10.1016/j.ajog.2015.02.016 (2015).

8 Asano, R. *et al.* Expression of erythropoietin messenger ribonucleic acid in wild-type MED12 uterine leiomyomas under estrogenic influence: new insights into related growth disparities. *Fertil Steril* **111**, 178-185 (2019).

9 Wu, X. *et al.* Subtype-Specific Tumor-Associated Fibroblasts Contribute to the Pathogenesis of Uterine Leiomyoma. *Cancer Res* **77**, 6891-6901 (2017).

10 George, J. W. *et al.* Integrated Epigenome, Exome, and Transcriptome Analyses Reveal Molecular Subtypes and Homeotic Transformation in Uterine Fibroids. *Cell reports* **29**, 4069-4085.e4066, doi:10.1016/j.celrep.2019.11.077 (2019).

11 Liu, X., Liu, Y., Zhao, J. & Liu, Y. Screening of potential biomarkers in uterine leiomyomas disease via gene expression profiling analysis. *Mol Med Rep* **17**, 6985-6996 (2018).

12 Kim, M. & Costello, J. DNA methylation: an epigenetic mark of cellular memory. *Exp Mol Med* **49**, e322, doi:10.1038/emm.2017.10 (2017).

13 Maekawa, R. *et al.* Aberrant DNA methylation suppresses expression of estrogen receptor 1 (ESR1) in ovarian endometrioma. *J Ovarian Res* **12**, 14, doi:10.1186/s13048-019-0489-1 (2019).

14 Maekawa, R. *et al.* Tissue-Specific Expression of Estrogen Receptor 1 Is Regulated by DNA Methylation in a T-DMR. *Mol Endocrinol* **30**, 335-347 (2016).

15 Maekawa, R. *et al.* Genome-wide DNA methylation analysis reveals a potential mechanism for the pathogenesis and development of uterine leiomyomas. *PLoS One* **8**, e66632, doi:10.1371/journal.pone.0066632 (2013).

16 Sato, S. *et al.* Identification of uterine leiomyoma-specific marker genes based on DNA methylation and their clinical application. *Sci Rep* **6**, 30652, doi:10.1038/srep30652 (2016).

17 Maekawa, R. *et al.* Disease-dependent differently methylated regions (D-DMRs) of DNA are enriched on the X chromosome in uterine leiomyoma. *J Reprod Dev* **57**, 604-612 (2011).

18 Sato, S. *et al.* Potential mechanisms of aberrant DNA hypomethylation on the x chromosome in uterine leiomyomas. *J Reprod Dev* **60**, 47-54 (2014).

19 Sato, S. *et al.* SATB2 and NGR1: potential upstream regulatory factors in uterine leiomyomas. *J Assist Reprod Genet* **36**, 2385-2397 (2019).

20 Zhang, B. & Horvath, S. A general framework for weighted gene co-expression network analysis. *Stat Appl Genet Mol Biol* **4**, Article17, doi:10.2202/1544-6115.1128 (2005).

21 Langfelder, P. & Horvath, S. WGCNA: an R package for weighted correlation network analysis. *BMC Bioinformatics* **9**, 559, doi:10.1186/1471-2105-9-559 (2008).

22 Borahay, M. A., Al-Hendy, A., Kilic, G. S. & Boehning, D. Signaling Pathways in Leiomyoma: Understanding Pathobiology and Implications for Therapy. *Mol Med* **21**, 242-256, (2015).

23 Ciebiera, M. *et al.* Role of Transforming Growth Factor beta in Uterine Fibroid Biology. *Int J Mol Sci* **18**, doi:10.3390/ijms18112435 (2017).

24 Reis, F. M., Bloise, E. & Ortiga-Carvalho, T. M. Hormones and pathogenesis of uterine fibroids. *Best Pract Res Clin Obstet Gynaecol* **34**, 13-24 (2016).

25 Zannotti, A. *et al.* Macrophages and Immune Responses in Uterine Fibroids. *Cells* **10**,

doi:10.3390/cells10050982 (2021).

26 Leppert, P. C., Catherino, W. H. & Segars, J. H. A new hypothesis about the origin of uterine fibroids based on gene expression profiling with microarrays. *Am J Obstet Gynecol* **195**, 415-420, (2006).

27 Orciani, M. *et al.* Chronic Inflammation May Enhance Leiomyoma Development by the Involvement of Progenitor Cells. *Stem Cells Int* **2018**, 1716246, doi:10.1155/2018/1716246 (2018).

28 Fletcher, N. M. *et al.* Uterine fibroids are characterized by an impaired antioxidant cellular system: potential role of hypoxia in the pathophysiology of uterine fibroids. *J Assist Reprod Genet* **30**, 969-974, (2013).

29 Bertsch, E. *et al.* MED12 and HMGA2 mutations: two independent genetic events in uterine leiomyoma and leiomyosarcoma. *Modern pathology : an official journal of the United States and Canadian Academy of Pathology, Inc* **27**, 1144-1153 (2014).

30 Mehine, M., Makinen, N., Heinonen, H. R., Aaltonen, L. A. & Vahteristo, P. Genomics of uterine leiomyomas: insights from high-throughput sequencing. *Fertil Steril* **102**, 621-629 (2014).

31 Mello, J. B. H. *et al.* MicroRNAs involved in the HMGA2 deregulation and its co-occurrence with MED12 mutation in uterine leiomyoma. *Mol Hum Reprod* **24**, 556-563 (2018).

32 Maekawa, R. *et al.* Genome-wide DNA methylation analysis revealed stable DNA methylation status during decidualization in human endometrial stromal cells. *BMC Genomics* **20**, 324, doi:10.1186/s12864-019-5695-0 (2019).

33 Yamagata, Y. *et al.* Genome-wide DNA methylation profiling in cultured eutopic and ectopic endometrial

stromal cells. *PLoS One* **9**, e83612, doi:10.1371/journal.pone.0083612 (2014).

34 Mihara, Y. *et al.* An Integrated Genomic Approach Identifies HOXC8 as an Upstream Regulator in Ovarian Endometrioma. *J Clin Endocrinol Metab* **105**, doi:10.1210/clinem/dgaa618 (2020).

35 Love, M. I., Huber, W. & Anders, S. Moderated estimation of fold change and dispersion for RNA-seq data with DESeq2. *Genome biology* **15**, 550, doi:10.1186/s13059-014-0550-8 (2014).

36 Yu, G., Wang, L. G., Han, Y. & He, Q. Y. clusterProfiler: an R package for comparing biological themes among gene clusters. *OMICS* **16**, 284-287 (2012).

37 Huang da, W. *et al.* DAVID Bioinformatics Resources: expanded annotation database and novel algorithms to better extract biology from large gene lists. *Nucleic Acids Res* **35**, W169-175, doi:10.1093/nar/gkm415 (2007).

38 R Core Team. R: A language and environment for statistical computing. (2021).

39 Supek, F., Bosnjak, M., Skunca, N. & Smuc, T. REVIGO summarizes and visualizes long lists of gene ontology terms. *PLoS One* **6**, e21800, doi:10.1371/journal.pone.0021800 (2011).

Acknowledgments

This work was supported in part by JSPS KAKENHI (Grant Number 19K09803, 21K09495, 20K18222, 20K09601, and 20H03825).

Author contributions

RM and NS recruited patients, secured their biological samples, performed data analysis, and wrote the manuscripts. RM and NS conceived and designed the study. TT, TS, TK, and KS participated in the experiments and analyses. All authors participated in the writing and approved the final version of the manuscript.

Competing interests

The authors declare no competing interests.

Data availability

The data underlying this article are available in the Dryad Digital Repository at https://doi.org/10.5061/dryad.sn02v6x4d (please use the following link during review process https://datadryad.org/stash/share/eyqm-aWxXAEWt2-CK7nZ4aukRX40dF8WLoz1xnw8WLc).

572 Figure legends

573 Figure 1. DNA methylation profiling of the MED12m-positive and -negative uterine fibroids, and
574 myometrium.

575 a. DNA methylation profiles of the MED12m-positive and -negative uterine fibroids, and myometrium were
576 compared using hierarchical clustering analyses. Distances of DNA methylation pattern are indicated as
577 height. Each color indicates the myometrium (light blue), the MED12m-positive uterine fibroids (red), and
578 the MED12m-negative uterine fibroids (green). The MED12m-negative uterine fibroids were further
579 classified into three different clusters, Subtype-1, Subtye-2, and Subtype-3. b. Chromosomal distribution
580 of hyper- or hypomethylated CpGs in the MED12m-positive and -negative uterine fibroids (Subtype-1, -2,
581 and -3) compared to the myometrium are shown. The locations of CpG sites, which have $p<0.05$ and beta-
582 value difference >0.2 compared to the myometrium, are indicated with red (hypermethylated CpGs) or blue
583 (hypomethylated CpGs). Autosomal and sex chromosome numbers are shown on the top.

584 Figure 2. The scatterplot of GO terms in DEGs.

585 The plots and tables show the GO terms after the redundancy reduction in the MED12m-positive-increased
586 (a), -decreased (b), the MED12m-negative-increased (c), and -decreased (d) DEGs. The colors indicate the
587 log10(p-value) of the summarized GO terms. The size of the circle indicates the frequency of the GO term
588 in the underlying GO database. The circles of more general terms are plotted larger. The color and the
589 size of circles are plotted according to the default setting of REVIGO [39]. e. Summary of GO analysis in
590 the MED12m-positive and -negative uterine fibroids.

591 The specific terms to the MED12m-positive uterine fibroids, the MED12m-negative uterine fibroids, and
592 commonly detected terms are shown. Red and blue mean higher and lower expression compared to the
593 myometrium

594 Figure 3. Expression levels of representative genes in the detected biophysical processes.

595 Representative genes in commonly (a) or oppositely (b) activated/deactivated processes between the
596 MED12m-positive and -negative uterine fibroids were indicated. a, $p<0.01$ (myometrium (n=6) vs.
597 MED12m-positive uterine fibroids (n=6)). b, $p<0.01$ (myometrium (n=6) vs. MED12m-negative uterine
598 fibroids (n=9)).

599 Figure 4. Enriched GO terms identified by weighted gene co-expression network analysis (WGCNA) in the
600 MED12m-positive and -negative uterine fibroids.

601 Twenty-six and 14 COGs groups in the MED12m-positive and -negative uterine fibroids, respectively, were
602 introduced into the KEGG pathway and GO enrichment analyses. Three and five COGs groups in the
603 MED12m-positive and -negative uterine fibroids were significantly enriched with GO terms. The other 23
604 and 9 COGs groups in the MED12m-positive and -negative uterine fibroids, respectively, were not
605 significantly enriched with GO terms. The ratio of the number of identified genes to all genes in each term
606 is shown as "geneRatio". P-values were adjusted with the BH method by clusterProfiler [36] and indicated
607 with colors.

608 Figure 5. Histological examination in the uterine fibroids and myometrium.

609 a. Immunofluorescent staining for collagen fibers in the MED12m-positive, -negative uterine fibroids, and

610 myometrium. Collagen fibers are detected as blue by a trichrome staining kit (TRM-1, ScyTec
611 Laboratories inc). b. Boxplots show the occupation rate of collagen fiber. The collagen fiber area was
612 quantified by Image J. The percentage per view field was calculated on 15 randomly chosen areas at x200
613 magnification, and average percentages were indicated in each tissue section. *, $p < 0.05$. c.
614 Immunofluorescent staining for smooth muscle cells (αSMA, green) and vascular endothelial cells (CD31,
615 red) in the MED12m-positive, -negative uterine fibroids, and myometrium. d. Boxplots show the number
616 of blood vessels, which was counted by Image J. The number per view field was calculated on 5 randomly
617 chosen areas at x100 magnification, and the average numbers were indicated in each tissue section. *, $p <$
618 0.05. e. Immunofluorescent staining for smooth muscle cells (αSMA, red) and nucleus (DAPI, blue) in the
619 MED12m-positive, -negative uterine fibroids, and myometrium. The cells stained with αSMA were
620 considered as smooth muscle cells, whereas the cells that were not stained with αSMA was considered as
621 non-smooth muscle cells. f. Boxplots show the percentage of the smooth muscle cells in the smooth and
622 non-smooth muscle cells. The number per view field was calculated on 5 randomly chosen areas at x200
623 magnification, and the average numbers were indicated in each tissue section. *, $p < 0.05$.

624 Figure 6. DNA methylation and mRNA expression statuses of SATB2 and NRG1 genes.

625 a and b. The DNA methylation levels of SATB2 (a) and NRG1 (b) genes are shown in dot plots. The
626 vertical axis indicates the DNA methylation levels in the MED12m-positive uterine fibroids ($n = 9$), -
627 negative uterine fibroids ($n = 12$), and the corresponding myometrium. The DNA methylation levels were
628 examined by COBRA and range from 0 to 100 %. c and d. The expression levels of SATB2 (c) and NRG1

(d) genes in the MED12m-positive uterine fibroids, -negative uterine fibroids, and the myometrium analyzed by qRT-PCR are shown in dot plots. The expression levels are corrected for myometrium expression as 1.

Table 1. COGs groups detected by WGCNA and the numbers of COGs groups with significant KEGG pathways and GO terms.

	total genes	genes assigned to COGs groups	genes without assignement to COGs groups	Number of detected COGs groups	Number COGs groups with significant GO terms
MED12m-positive	19860	19859	1	26	3
MED12m-negative	19860	16183	3677	14	5

Table 2. Activated signalings of cell proliferation and anti-apoptosis in differentially expressed genes in uterine fibroids.

IPA pathway ($p < 0.05$)	MED12m-positive	MED12m-negative
Cell proliferation		
Wnt/β-catenin signaling	●	
HIF1α- signaling	●	
mTOR signaling	●	●
PI3K/AKT signaling	●	●
p70S6K signaling	●	●
STAT3 siganling	●	●
RANK signaling in osteoclasts	●	
PPARα/RXTα activation	●	
NF-κB signaling	●	
RAR activation	●	●
PXR/RXR activation		●
HER-2/ErbB signaling		●
ERK/MAPK siganling		●
LPS-stimulated MAPK signaling		●
Anti-apoptosis		
14-3-3mediated signaling	●	
PI3K/AKT signaling	●	●
p70S6K signaling	●	●
PAK signaling		●
IGF-1 signaling		●

Differentially expressed genes compared to the myometrium (the DEGs) in the MED12m-positive and -negative uterine fibroids were applied to KEGG pathway analysis in IPA, respectively. Detected pathways with $p<0.05$ were considered significant enrichment. Activated signaling pathways related to cell proliferation and anti-apoptosis were indicated.

Figures

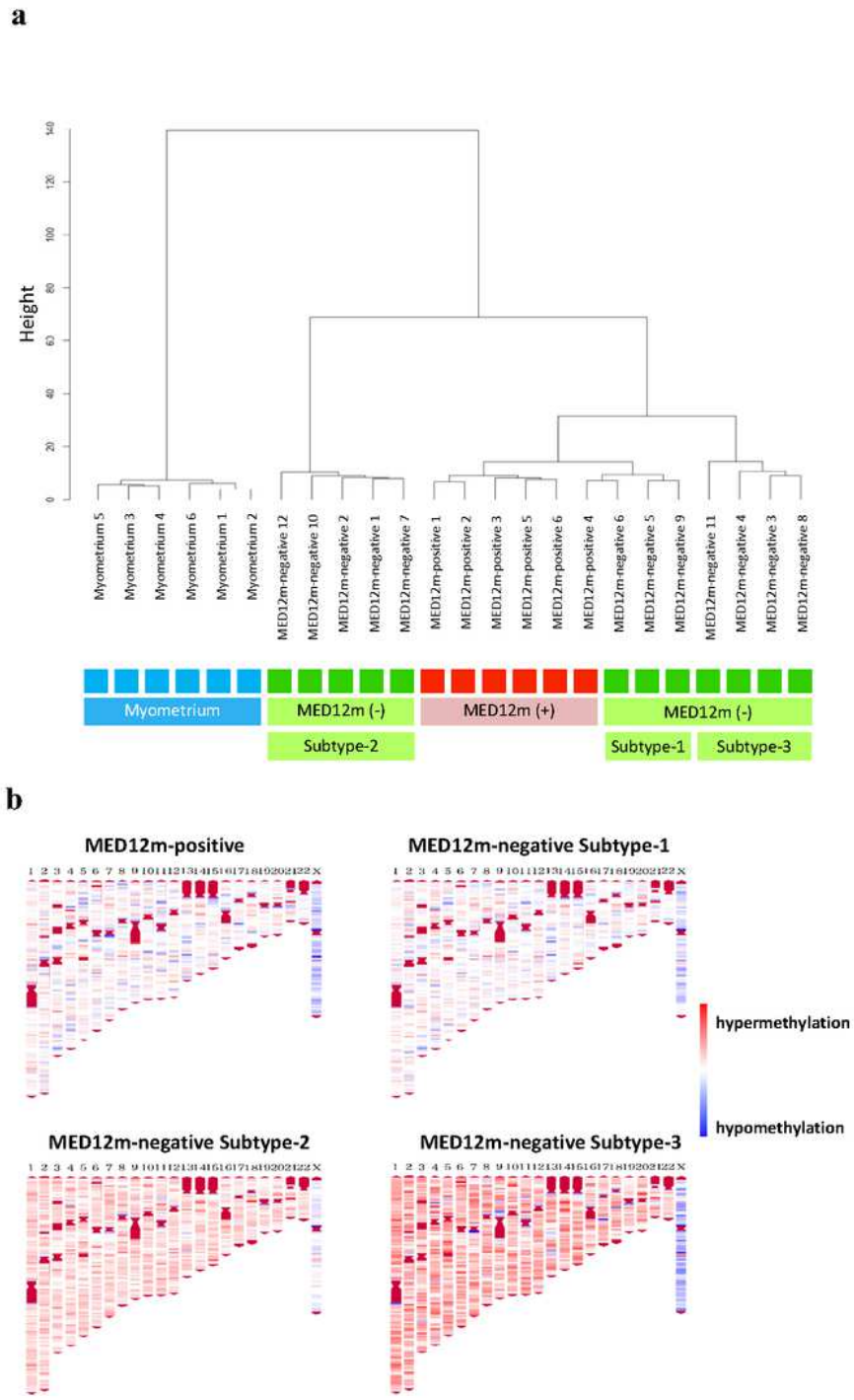

Figure 1

DNA methylation profiling of the MED12m-positive and -negative uterine fibroids, and myometrium. a. DNA methylation profiles of the MED12m-positive and -negative uterine fibroids, and myometrium were compared using hierarchical clustering analyses. Distances of DNA methylation pattern are indicated as

height. Each color indicates the myometrium (light blue), the MED12m-positive uterine fibroids (red), and the MED12m-negative uterine fibroids (green). The MED12m-negative uterine fibroids were further classified into three different clusters, Subtype-1, Subtye-2, and Subtype-3. b. Chromosomal distribution of hyper- or hypomethylated CpGs in the MED12m-positive and -negative uterine fibroids (Subtype-1, -2, and -3) compared to the myometrium are shown. The locations of CpG sites, which have $p<0.05$ and beta value difference >0.2 compared to the myometrium, are indicated with red (hypermethylated CpGs) or blue (hypomethylated CpGs). Autosomal and sex chromosome numbers are shown on the top.

a

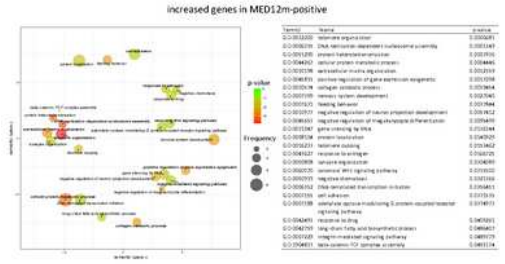

b

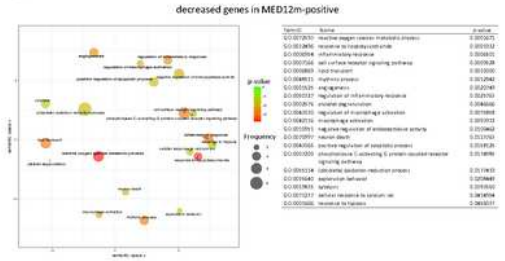

Figure 2 (continued)

c

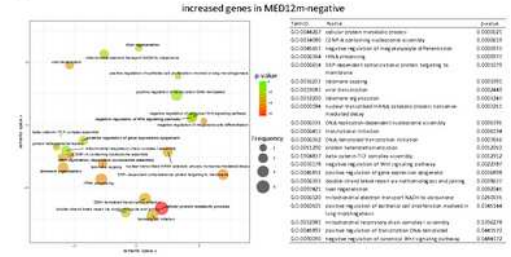

d

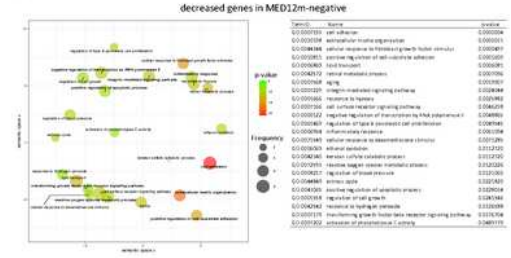

Figure 2 (continued)

e

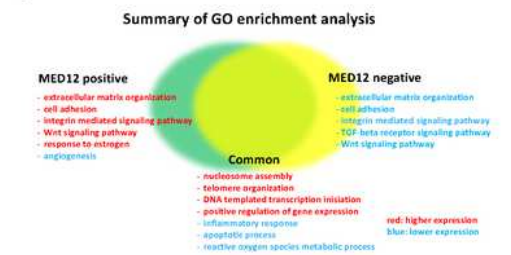

Figure 2

The scatterplot of GO terms in DEGs. The plots and tables show the GO terms after the redundancy reduction in the MED12m-positive-increased (a), -decreased (b), the MED12m-negative-increased (c), and -decreased (d) DEGs. The colors indicate the log10(p-value) of the summarized GO terms. The size of the circle indicates the frequency of the GO term in the underlying GO database. The circles of more general terms are plotted larger. The color and the size of circles are plotted according to the default setting of REVIGO 39. e. Summary of GO analysis in the MED12m-positive and -negative uterine fibroids. The specific terms to the MED12m-positive uterine fibroids, the MED12m-591 negative uterine fibroids, and commonly detected terms are shown. Red and blue mean higher and lower expression compared to the myometrium

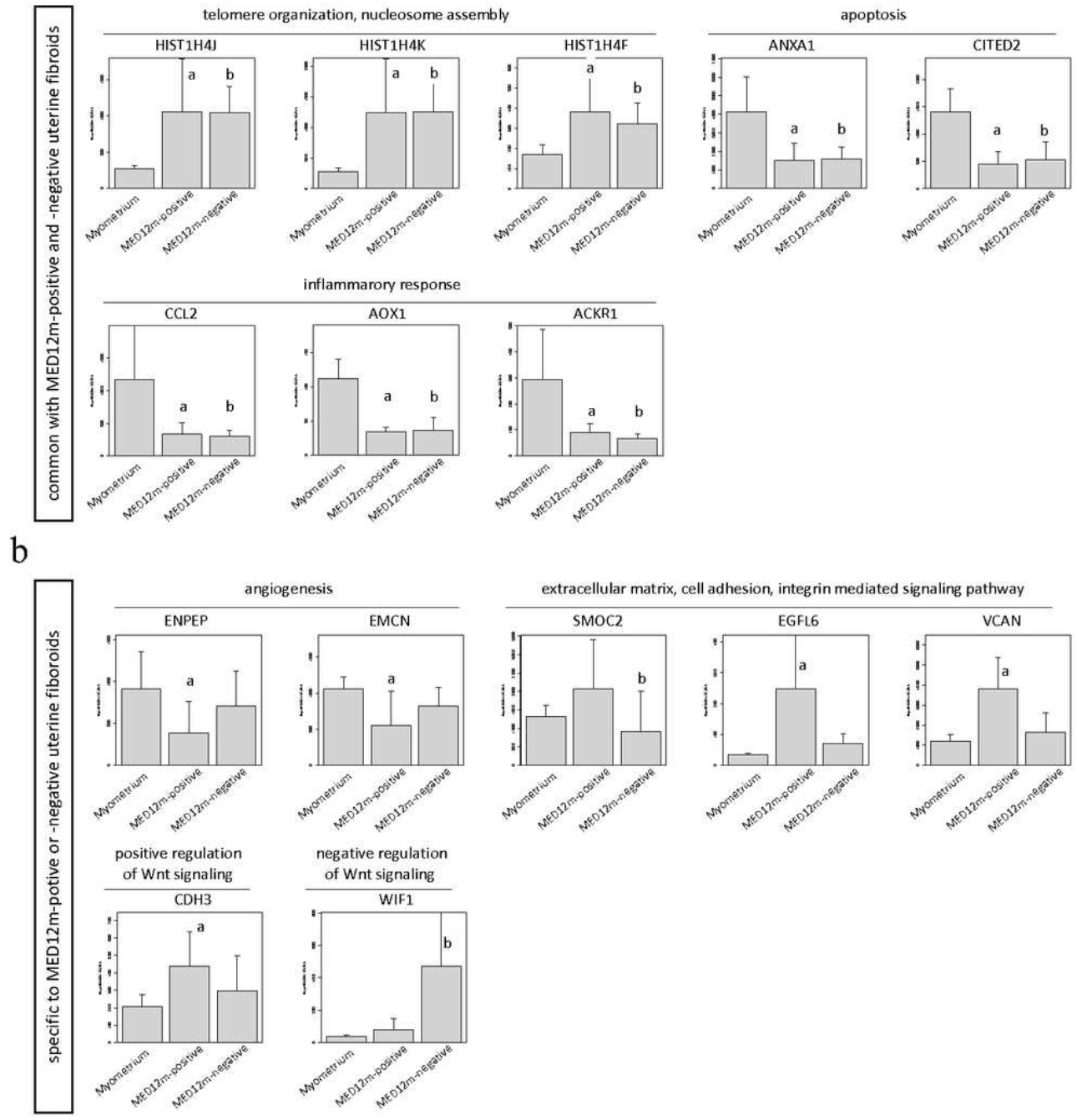

Figure 3

Expression levels of representative genes in the detected biophysical processes. Representative genes in commonly (a) or oppositely (b) activated/deactivated processes between the MED12m-positive and -negative uterine fibroids were indicated. a, $p<0.01$ (myometrium (n=6) vs. MED12m-positive uterine fibroids (n=6)). b, $p<0.01$ (myometrium (n=6) vs. MED12m-negative uterine fibroids (n=9)).

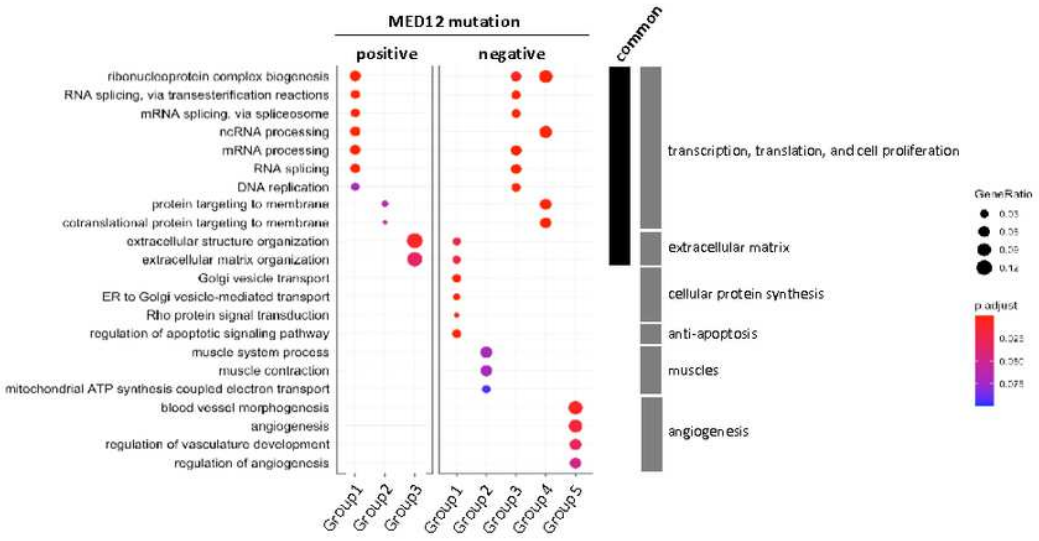

Figure 4

Enriched GO terms identified by weighted gene co-expression network analysis (WGCNA) in the MED12m-positive and -negative uterine fibroids. Twenty-six and 14 COGs groups in the MED12m-positive and -negative uterine fibroids, respectively, were introduced into the KEGG pathway and GO enrichment analyses. Three and five COGs groups in the MED12m-positive and -negative uterine fibroids were significantly enriched with GO terms. The other 23 and 9 COGs groups in the MED12m-positive and -negative uterine fibroids, respectively, were not significantly enriched with GO terms. The ratio of the number of identified genes to all genes in each term is shown as "geneRatio". P-values were adjusted with the BH method by clusterProfiler 36 and indicated with colors.

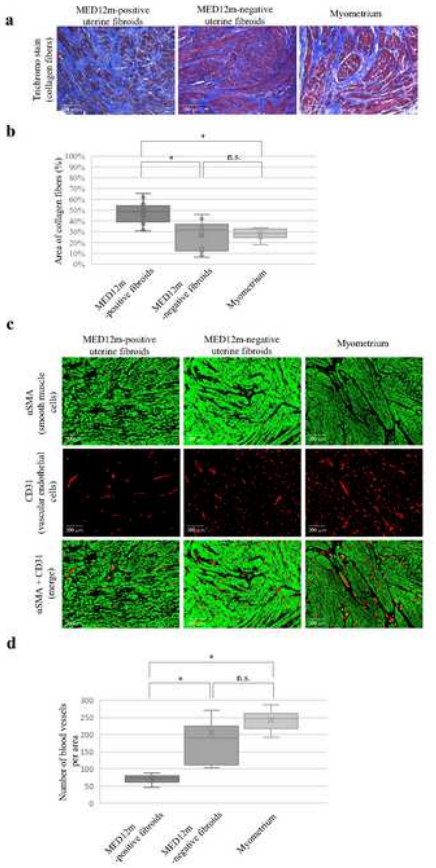

Figure 5 (continued)

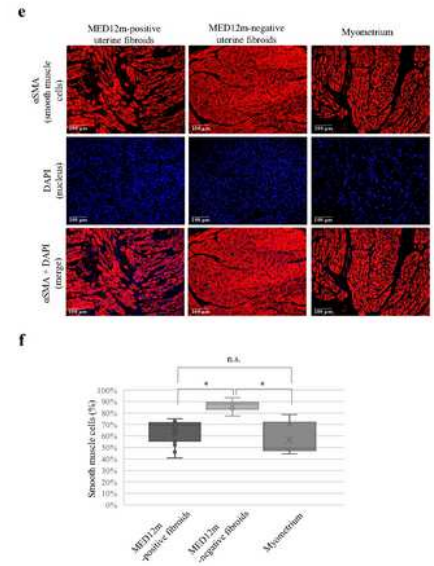

Figure 5

Histological examination in the uterine fibroids and myometrium. a. Immunofluorescent staining for collagen fibers in the MED12m-positive, -negative uterine fibroids, and myometrium. Collagen fibers are detected as blue by a trichrome staining kit (TRM-1, ScyTec Laboratories inc). b. Boxplots show the occupation rate of collagen fiber. The collagen fiber area was quantified by Image J. The percentage per view field was calculated on 15 randomly chosen areas at x200 magnification, and average percentages

were indicated in each tissue section. *, $p < 0.05$. c. Immunofluorescent staining for smooth muscle cells (αSMA, green) and vascular endothelial cells (CD31, red) in the MED12m-positive, -negative uterine fibroids, and myometrium. d. Boxplots show the number of blood vessels, which was counted by Image J. The number per view field was calculated on 5 randomly chosen areas at x100 magnification, and the average numbers were indicated in each tissue section. *, $p < 0.05$. e. Immunofluorescent staining for smooth muscle cells (αSMA, red) and nucleus (DAPI, blue) in the MED12m-positive, -negative uterine fibroids, and myometrium. The cells stained with αSMA were considered as smooth muscle cells, whereas the cells that were not stained with αSMA was considered as non-smooth muscle cells. f. Boxplots show the percentage of the smooth muscle cells in the smooth and non-smooth muscle cells. The number per view field was calculated on 5 randomly chosen areas at x200 magnification, and the average numbers were indicated in each tissue section. *, $p < 0.05$.

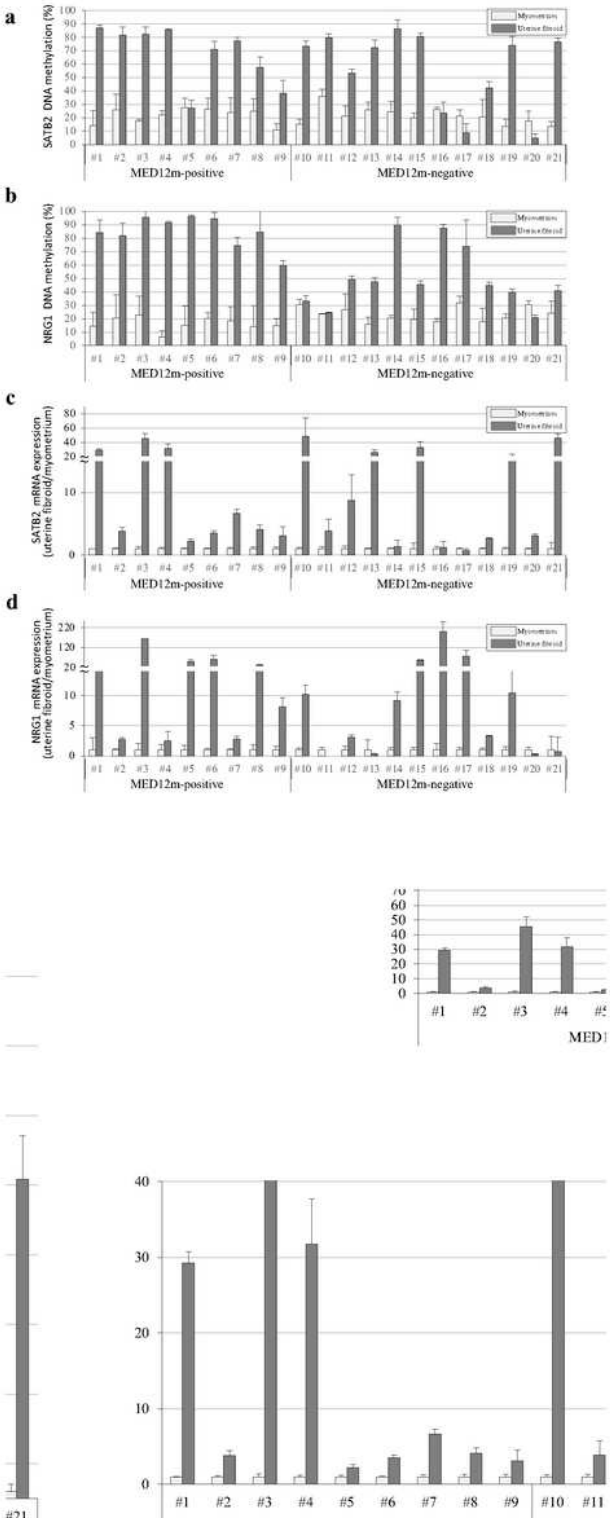

Figure 6

DNA methylation and mRNA expression statuses of SATB2 and NRG1 genes. a and b. The DNA methylation levels of SATB2 (a) and NRG1 (b) genes are shown in dot plots. The vertical axis indicates the DNA methylation levels in the MED12m-positive uterine fibroids (n = 9), - negative uterine fibroids (n = 12), and the corresponding myometrium. The DNA methylation levels were examined by COBRA and range from 0 to 100 %. c and d. The expression levels of SATB2 (c) and NRG1 (d) genes in the MED12m-

positive uterine fibroids, -negative uterine fibroids, and the myometrium analyzed by qRT-PCR are shown in dot plots. The expression levels are corrected for myometrium expression as 1.

Supplementary Files

This is a list of supplementary files associated with this preprint. Click to download.

- SupplementalMaterials.pdf